Article

Not peer-reviewed version

Effect of Chitin Nanocrystals Deacetylation on a Nature-Mimicking Interface in Carbon Fiber Composites

A. M. Abdel-Mohsen , R. M. Abdel-Rahman , L. Kalina , V Vishakha , Ludmila Kaprálková , Pavel Nemecek , Josef Jancar , Ivan Kelnar *

Posted Date: 2 February 2024

doi: 10.20944/preprints202402.0102.v1

Keywords: graphene oxide; chitin nanocrystals; delamination resistance; tough interface; electrophoresis; carbon fiber composite

 doi:10.20944/preprints202402.0102.v1

Article

Effect of Chitin Nanocrystals Deacetylation on a Nature-Mimicking Interface in Carbon Fiber Composites

A. M. Abdel-Mohsen [1], R. M. Abdel-Rahman [1], L. Kalina [2], V. Vishakha [3], L. Kaprálková [1], P. Němeček [1], J. Jančář [2,3] and I. Kelnar [1,*]

[1] Institute of Macromolecular Chemistry, Czech Academy of Sciences, Heyrovského nám. 2, Praha 162 00, Czech Republic

[2] Faculty of Chemistry, Materials Research Center, Brno University of Technology, Purkyňova 464/118, Brno 612 00, Czech Republic

[3] CEITEC-Central European Institute of Technology, Brno University of Technology, Purkyňova 656/123, Brno 612 00, Czech Republic

* Correspondence: kelnar@imc.cas.cz

Abstract: The formation of a rigid tough interface based on a nacre-like structure in carbon fiber (CF) composites is a promising way to eliminate low delamination resistance. An effective method of coating CFs is electrophoretic deposition (EPD), which, in the case of dissimilar components like graphene oxide (GO) and polymeric glue, usually requires their chemical bonding/ strong interactions. In this work, we focus on chitin nanocrystals (ChNCs), leading to an excellent mechanical performance of artificial nacre, where favorable interactions and bonding with GO were controlled by degrees of deacetylation (5, 15 and 30 %). We have prepared coatings based on GO/ChNCs adducts with 95/5, 90/10,50/50 and 25/75 ratios using optimized EPD conditions (pH, concentration, voltage and time). The prepared materials were characterized using FTIR, TEM, XPS, SEM, DLS, and XRD. SEM evaluation indicates the formation of a homogeneous interlayer, which possesses a fair ability of chemical bonding with the epoxy matrix. Short beam testing of epoxy matrix composites indicates that coating does not decrease stiffness and its relatively low dependence on composition. Therefore, all coatings are promising for a detailed study of delamination resistance using laminate samples. Moreover, facile EPD from water solution/ suspension has a fair potential for industrial applications.

Keywords: graphene oxide; chitin nanocrystals; delamination resistance; tough interface; electrophoresis; carbon fiber composite

1. Introduction

It is now well accepted that combinations of carbon nanoplatelets (CN) with small amounts of various polymers [1–3] and polysaccharides [4] may form nature-mimicking materials with unique compact structures and impressive mechanical parameters, which can exceed those of nacre, that is, the natural 'gold standard' of strong tough material [5,6].

It was recently demonstrated that analogous materials with unique performance (deformation mechanism) can be obtained by combining CN with suitable organic anisotropic nanoparticles, mostly nanofibrils/whiskers. An example is a system containing reduced GO and covalently linked cellulose nanofibrils (CNC) [7] with a typical composition for nacres (80%-97% GO), some other nanoplatelet/CNC combinations [7–12] or nanofibrillated cellulose/CN/ diblock protein system [13]. Other high-performance nature mimicking materials are based on different silk fibroin/GO combinations [14,15].

So far, only one study has reported the application of chitin nanocrystals (ChNCs) in a system combining silk nanofibril (SNF), hydroxyapatite nanocrystals and ChNCs [16]. These results are

 doi:10.20944/preprints202402.0102.v1

consistent with the fact that nacre is a ternary composite consisting of aragonite platelets, nanofibrillar chitin and protein [5]. In this respect, considering the prime importance of interactions/linking between components [7,10], we can consider the promising potential of nanosized polar amino functionalized ChNCs with a favorable aspect ratio (AR) to form GO-based nacre analogs. Furthermore, ChNC preparation is easier than nanofibrillated cellulose, with further benefits in using waste material [17,18].

ChNCs, mostly prepared from chitin, is a rigid crystalline nanofibre with a Young modulus of 40–80 GPa. It comprises repeating units of glucosamine and *N*-acetylglucosamine that contain reactive groups, i.e., amines. Thus, chitin has more significant potential for chemical modifications than cellulose. Chitin nanocrystals can be produced in a relatively wide range of length, diameter, charge density, type of charge, and crystallinity through various top-down procedures [17–20].

In the area of fibrous composites, different nanoparticles, mainly CN and CNT, are applied to modify the interface as a single coating. This includes electrophoretic deposition (EPD) [21,22] and CVD [23], components of sizing [24] or even direct linking to CF to form hierarchical hairy fibers [25–27].

In the case of cellulose nanocrystals (CNC) and microfibrils [28–30] or silane-modified CNC [30], various dip coatings of glass fibers and carbon fibers (CF) are reported, while aramid fibers were coated with aramid microfibers by EPD [30,31] or by dip coating of aramid microfibers/graphene combination [32]. This modification of the fiber surface provides the benefit of enhanced roughness, increasing frictional adhesion components, and higher interphase modulus. At the same time, an important deficiency of composites, low resistance against impact-delamination [33] (interlaminar cracking) can be eliminated by a tough, usually low modulus interface [34] due to an increase in impact energy release. However, this leads to a significant reduction in stiffness [35].

Fair mechanical properties, including increased interlaminar shear strength (ILSS), were found with a more rigid coating by CNC [28,29]. At the same time, solution by various methods that improve the toughness of the matrix brings processing limitations and reduction of resistance against fiber buckling [36]. On the basis of the above facts, we consider the important role of the tough rigid interfaces using nature-mimicking nacre-like structures. So far, rigid-soft structures based on CNT modified with poly(ethylene glycol)methylether [37] and CNT/PEI combination [37] have been reported. However, unlike the comparable effect in single coating using GO or CNT [38] to enhance interfacial properties, the ability of tubular nanoelements to form complex structures and thus rigid tough interface is limited. In the case of 2D platelets, the potential to create effective ordered structures is more marked [38].

So far, only some layer-by-layer deposition of alternating polymer/nanoparticle (NP) layers has been reported. Examples are layers of polydopamine (PDA)/GO [39,40], PDA/ POSS [41] or PDA/NiOH platelets [42]. NP grafting to the deposited polymeric layer [43] is also reported.

Recently, we have prepared CF coatings using nacre-like interlayers by EPD of PDA coated or some polymer-grafted GO combinations showing an excellent ability to enhance ILSS without loss of stiffness [37]. To control the composition of EPD coatings in the two-component system, grafting of aminated polymer to GO or borate-mediated interactions/bonding of hydroxyl-containing PVA and CMC was necessary. Therefore, this study is aimed at highlighting the potential of alternative nacre-like coatings of carbon fibers based on GO with attached chitin nanocrystals (GO/ChNCs adducts) to upgrade epoxy/fiber composites together with a thorough study of the effect of ChNCs parameters and adduct composition on electrophoretic deposition of multiscale rigid tough hierarchical interphase.

2. Experimental part

2.1. Materials

Epoxy resin LG700 based on diglycidyl ether of bisphenol A (DGEBA) + hardener HG737, (GRM Systems, s.r.o.). Chitin flakes, 1-ethyl-3-(3-dimethylaminopropyl) carbodiimide hydrochloride (EDC), N-hydroxysuccinimide (NHS) were purchased from Sigma Aldrich (Praha, Czech Republic),

 doi:10.20944/preprints202402.0102.v1

graphite flakes (Graphite Týn, Czech Rep.); carbon fiber (CF) roving yarn filament Torayca T700SC 12k (GRM Systems, s.r.o.).

2.2. Preparation of graphene oxide (GO)

The modified Hummer's method [44] was used: briefly, 95 ml of concentrated sulfuric acid and 2 g of $NaNO_3$ were added to 4 g of graphite flakes in an ice bath. 12g of KMnO4 was slowly added and the mixture was stored at 35 ° C for 100 min. Then 184 ml of water was added while the temperature increased to ~95 °C. After 15 min, 420 ml of water with 5 ml of 30% H_2O_2 was added. The residue was washed with a mixture of water, 35 % HCl, and ethanol by centrifugation. The oxygen content was ~ 40 %. The final ~2 % water suspension was delaminated using a Bandelin 200W sonicator with 30 % amplitude for 15 min.

2.3. Preparation of Chitin Nanocrystals (ChNCs)

Chitin nanocrystals (ChNC) with different degrees of deacetylation (DDA) were prepared according to our previous works [18,45]. Briefly, Chitin nanocrystals were synthesized by an acid hydrolysis process using HCl (5 M) for 6 h at 90 °C, and the solid to medium solution ratio was approximately (1/100). The nanocrystals were obtained after centrifugation at 7500 rpm for 30 min at room temperature. ChNCs were dialyzed using a cellulose membrane cut (12-14 KDa) for one week at room temperature using deionized water changed every 12 h until pH reached 4.5. ChNCs were stored at 4 ° C in a refrigerator until further use. The DDA of ChNCs was 5, 15, and 30 % DDA from ss-NMR, respectively.

2.4. GO/ChNCs adduct synthesis

A certain amount (0.5 %) of GO was dispersed in deionized water. Then 50/25 mM of EDC / NGS was added to the GO with stirring for 2 h at room temperature to activate the carboxylic and epoxide groups of the GO. ChNCs with different degrees of deacetylation (5, 15, 30 % DDA) were added to the GO suspension drop by drop with stirring for 5 h at room temperature to obtain GO/ChNC adduct. The prepared materials were coded according to DDA (GO/$ChNCs_5$, GO/$ChNCs_{15}$ and GO/$ChNCs_{30}$ adducts). The materials obtained were dialyzed for 3 days at rt using deionized water.

2.5. Electrophoretic coating

Oxidized carbon fibers (OCF), prepared with nitric acid at 22 ° C for 120 h according to our previous work [46] were fixed between two stainless steel electrodes with a distance of ~10 mm. Electrophoretic deposition (EPD) proceeded according to the details in Table 1, also showing the composition of the respective adducts. After washing and drying, the composite bar of dimensions 3 x 6 x 18 mm containing 0.52 g of CF was prepared in a silicone mold. According to the literature, surface oxidation of CF has a negligible effect on the mechanical parameters of CF [47].

Table 1. Composition of GO/ChNCs adducts used for CF coating.

Number	*GO*	*ChNCs*	*DDA of ChNCs (%)*	*Abbreviation*
1	95	5	5	GO/$ChNCs_5$ adduct
2	90	10	5	GO/$ChNCs_5$ adduct
3	80	20	5	GO/$ChNCs_5$ adduct
4	50	50	5	GO/$ChNCs_5$ adduct
5	95	5	15	GO/$ChNCs_{15}$ adduct

 doi:10.20944/preprints202402.0102.v1

6	90	10	15	GO/ChNCs$_{15}$ adduct
7	80	20	15	GO/ChNCs$_{15}$ adduct
8	50	50	15	GO/ChNCs$_{15}$ adduct
9	95	5	30	GO/ChNCs$_{30}$ adduct
10	90	10	30	GO/ChNCs$_{30}$ adduct
11	80	20	30	GO/ChNCs$_{30}$ adduct
12	50	50	30	GO/ChNCs$_{30}$ adduct

2.6. Characterization of OCF coated with a GO / CHNC adduct

Attenuated total reflectance Fourier transform infrared spectroscopy (ATR-FTIR) was carried out using a Bruker Vertex V70 FTIR spectrometer and a Bruker Platinum ATR accessory with single reflection diamond crystal mount (Bruker Optik GmbH, Ettlingen, Germany). Samples were clamped directly against the diamond crystal using the platinum ATR sample clamp mechanism, ensuring consistent pressure per sample. Spectra were collected in the wavenumber region 3900–400 cm-1. Four data sets per sample were recorded, adding 128 interferograms per set. Spectra were measured at a scanner velocity of 40 kHz and a resolution of 4.0 cm-1. Using air as a reference, 128 background scans per sample were collected. The averaged spectra per sample were generated using the Bruker OPUS version 7.2 software, where all spectra were corrected for ATR and vector normalized throughout the spectrum. The second derivative spectra were calculated using a 13-point smoothing point Savitzky–Golay algorithm to better separate overlapping absorption bands within the Amide I band.

Short beam strength (SBS), also called interlaminar shear strength (ILSS), if applied to laminate samples, was determined according to ASTM D2344/D2344M using beam samples 3 x 6 x 18 mm; the three-point short-beam bending testing (span length 12 mm, span length to thickness ratio of 4) was performed with Instron 5800 apparatus using 1 mm/min crosshead speed. The morphology of native GO, ChNC, and GO/ChNCs adduct with different DDA (%) was visualized by transmission electron microscopy (TEM). The experiment was carried out with a Tecnai G2 spirit 12 electron microscope (FEI, Brno, Czech Republic). The surface of the fibers and fracture surfaces was observed using a scanning electron microscope (SEM, KEYENCE, VE7800) at 3 kV.

The rheological characterization of water suspensions (5 mg/ml) of native GO, ChNCs, and GO/ChNCs adduct was conducted at room temperature using ARES G2 Rheometer (TA Instruments). Parallel plates with cone/plate geometry (cone angle of 2 °, diameter of 40 mm) was used. Frequency sweep measurements were made in the range from 0.05–100 rad/s at a 1% strain amplitude.

X-ray photoelectron spectroscopy (XPS) was carried out with the Kratos Analytical Axis Ultra DLD system using a monochromatic Al Kα (hν = 1486.7 eV) operating at 75 W (5 mA, 15 kV). Spectra were obtained using an analysis area of ~300 × 700 μm. The Kratos charge neutralizer system was used for all analyses. The high-resolution spectra were measured with 0.1 eV step size and 20 eV pass energy. The instrument base pressure was 2·10-8 Pa. Spectra were analyzed using the CasaXPS software (version 2.3.15) by applying a Gaussian – Lawrence line shape for fitting and the ORIGIN 2016 software.

3. Results and discussions

3.1. Effect of DDA on GO/ChNC adduct formation

 doi:10.20944/preprints202402.0102.v1

The degree of deacetylation (%) affected the morphology of the ChNCs, as is obvious from (Figure 1a–c) showing the STEM of the ChNCs with different DDA (Figure 1 a–c). At lower DDA %, ChNCs show high aggregation with short crystal length (Figure 1a,f); by increasing the DDA from 15 to 30 %, the nanocrystals are slightly longer compared to 5 DDA (Figure 1b,c,f). Figure 1d shows the FTIR of ChNCs with different DDAs. The peak intensity ratio between the amino to acetamide groups increased with an increase in the amino group content from 5 to 30 DDA. Figure 1e shows the XRD of native chitin and ChNC within different DDA (5, 15, 30 %). From XRD, all the pristine chitin and ChNCs with different DDA exhibited six diffraction peaks at 2θ = 9.5 °, 12.8 °, 19.2 °, 20.71 °, 23.4 ° and 26.4 ° indexed as (020), (021), (110), (120), (130) and (013), respectively (Figure 1e), suggesting a crystalline structure of the α-chitin [18,48,49]. From Figure 1e, DDA did not significantly affect the crystallization of the ChNCs.

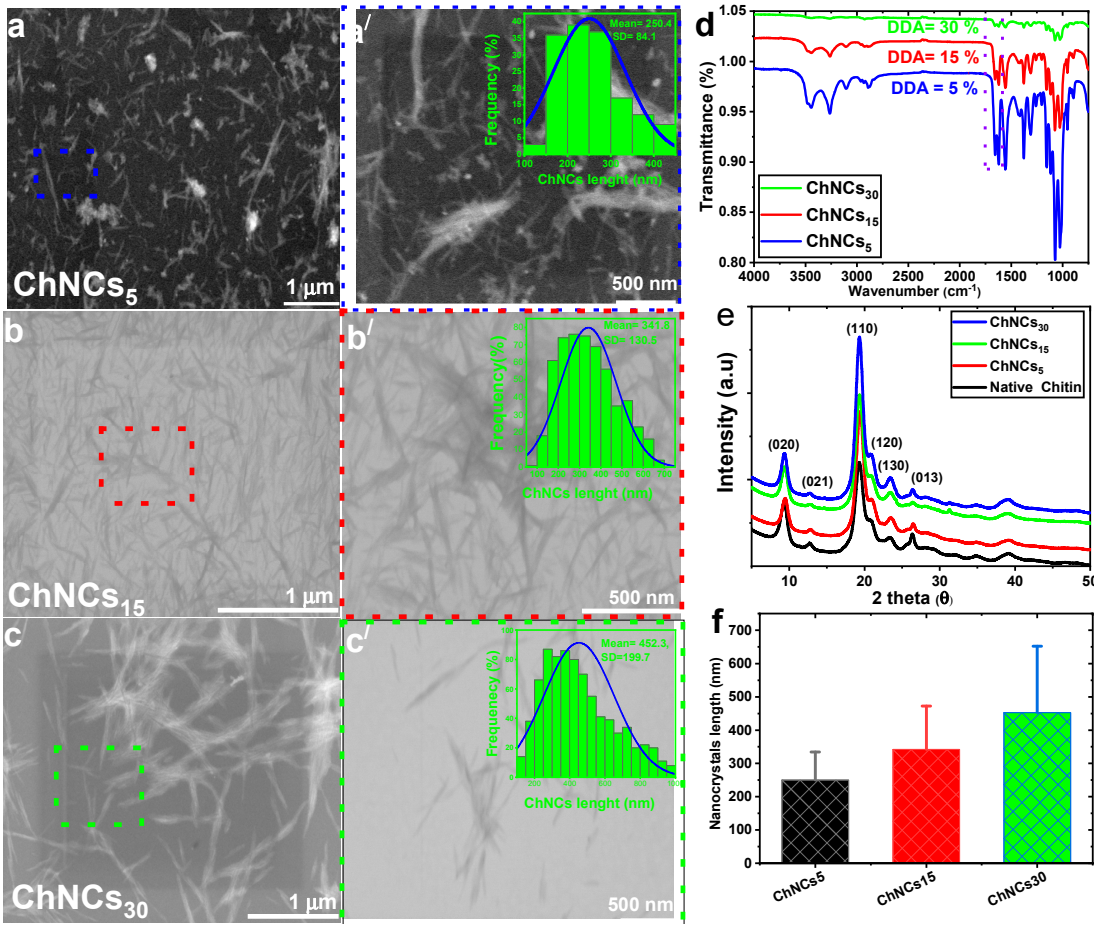

Figure 1. Representative STEM, FTIR, XRD, and histograms of ChNCs with different DDA (5, 15, 30 %).

Our preliminary results indicate that different charge densities and mobility/dimensions of both GO and ChNCs practically exclude the control of electrophoretic deposition (EPD) of these two-component systems, similar to other GO/polymer combinations [46]. Therefore, mutual bonding between components, using their functionality enabled by EDC/NHS, was applied to prepare GO/ChNCs adduct. When optimizing the EDC/GO/ChNCs/NHS ratio, amide and ester bonds between GO and ChNCs were created (Scheme 1a).

 doi:10.20944/preprints202402.0102.v1

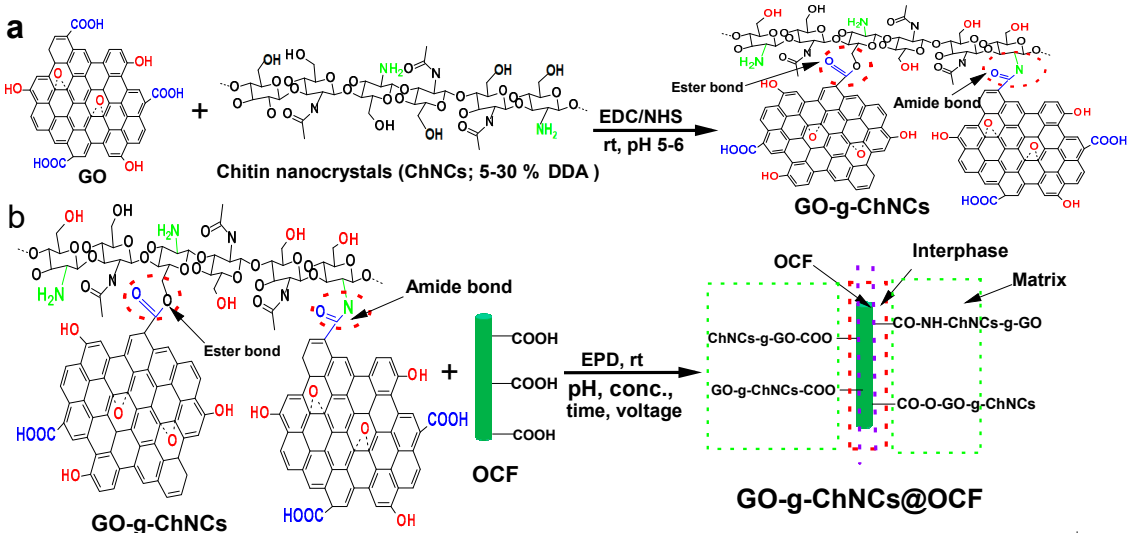

Scheme 1. Proposed chemical bonding and interaction between GO and the ChNCs and coating of OCF using the GO/ChNCs adduct. (a); linking of GO with ChNCs using EDC/NHS as crosslinker and catalyst, respectively; (b) coating of OCF using GO/ChNCs adduct (GO/ChNCs adduct@OCF).

From Figure 2 follows that the formation of a GO/ChNC polyelectrolyte complex and crosslinking reduced absorption for the OH and NH/NH_2 stretching vibration peaks. Furthermore, a new peak in the 1702 cm^{-1} region shows the esterification reaction between –COOH of graphene oxide (GO) and –OH of ChNCs. The peak of native GO at 1744 cm^{-1} corresponded to the physical ester bond between the COOH and OH GO groups that disappeared after grafting with $ChNCs_{30}$ (Figure 2a). Strong ionic interaction between carboxylic/epoxide of GO and amino/hydroxyl of ChNCs in the presence of an EDC/NHS cross-linker agent. (Figure 2a) caused that the peak intensity of the free amino groups with a 1557 cm-1 was weakened.

Figure 2b shows the XRD patterns of GO, $ChNCs_{30}$, and GO/ChNCs $adduct_{30}$. The diffraction peak of GO appeared at 2θ = 11.5°, which was associated with the characteristic peak (001 plane) of the interlayer structure of the GO nanosheets [50–52]. The $ChNCs_{30}$ diffraction peaks exhibited six diffraction peaks at 2θ = 9.5 °, 12.8 °, 19.2 °, 20.71 °, 23.4 ° and 26.4 ° indexed as (020), (021), (110), (120), (130) and (013), respectively. GO grafted with $ChNCs_{30}$ shows only broader diffraction peaks at 2θ = 20-30°, attributed to the presence of GO and ChNCs. Chitin nanocrystals are considered to be intercalated in the layered GO nanosheets.

Figure 2c shows the DLS of the native GO, GO/$ChNCs_5$ adduct, and GO/$ChNCs_{30}$ adduct. The size distribution of the native GO was about 90 nm, whereas for the GO / ChNCs5 adduct it decreased to 55 nm. At higher DDA, the size distribution of the adduct was about 150 nm. This corresponds to size of the ChNCs increasing with increased DDA from 5 to 30 % (Figure 1).

Interestingly, rheological characterization of water suspensions (Figure S1a) indicate substantially improved viscosity for adducts compared to both constituents with the highest value for adducts containing 75 % ChNC. This indicates the important effect of the adduct composition on its size, shape, and interactions.

 doi:10.20944/preprints202402.0102.v1

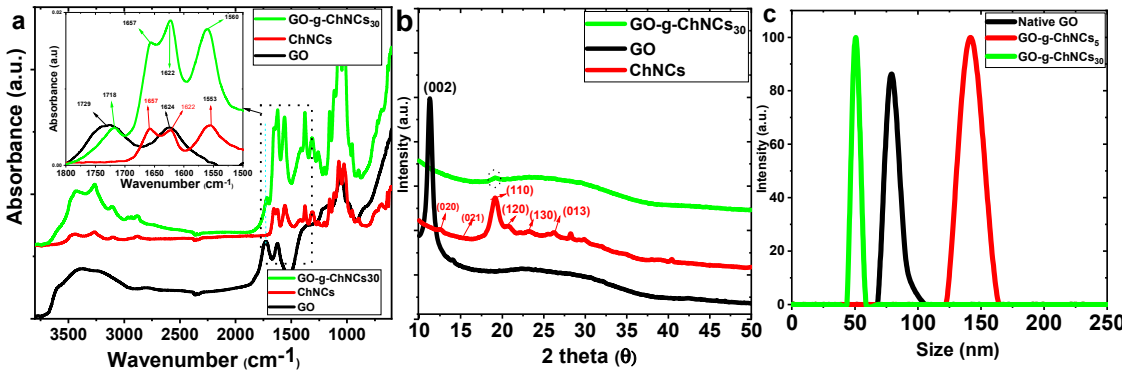

Figure 2. FTIR (a), XRD (b), DLS (c) of native components and their adducts.

Figure 3 shows fine ChNCs (Figure 3a,b) and a very thin layer of GO with a smooth surface (Figure 3c,d). The GO/ChNCs adduct shows a layered structure with larger thicknes against GO indicating adduct formation (Figure 3e,f).

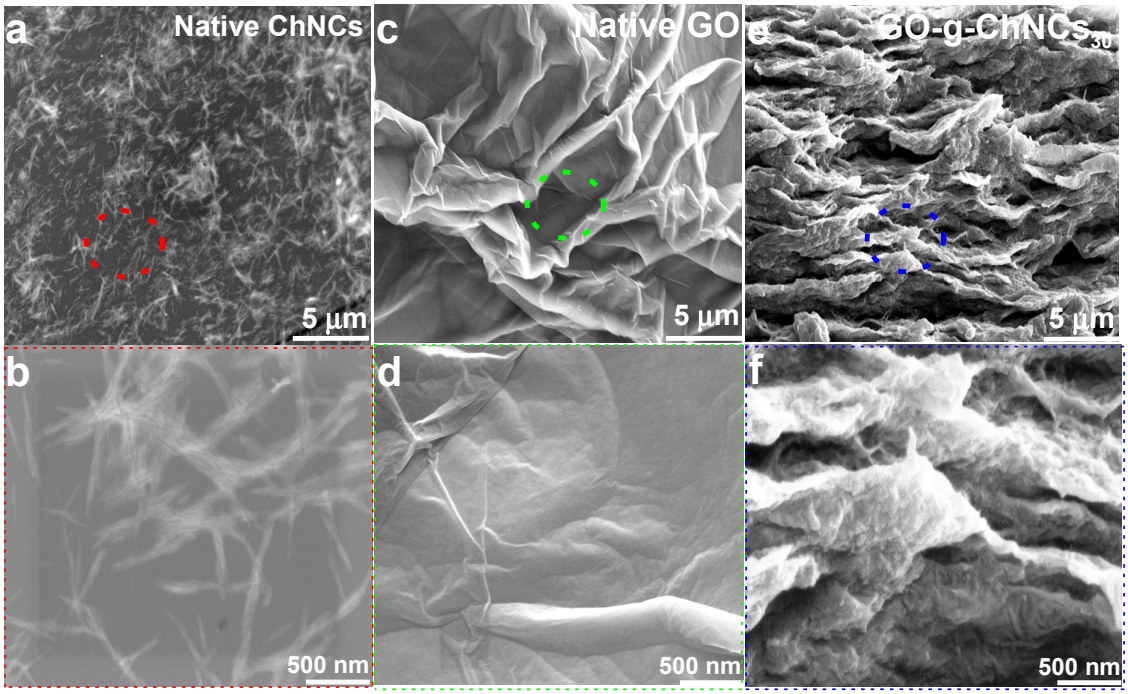

Figure 3. Representative SEM images of native ChNCs, GO and GO/ChNCs30 adduct after freeze-drying.

From XPS analysis of the adduct composition (Figure 4) it follows that only C, O, and N were detected from the broad spectra of oxidized carbon fibers (OCF). OCF C 1 shows different binding energies of -C=C, -C-C, -C-OH, -C-O, -COO, at 284.26 284.96, 286.03,286.9 and 288.2. Ev. From the C 1s and O 1s data, we can confirm that the carbon fibers were oxidized using nitric acid. Due to the high concentration of nitric acid used to oxidize the carbon fiber, a partial nitration reaction was observed in N 1 of oxidized carbon fibers (Figure 4). The broad XPS spectrum of native ChNCs shows expected signals for C, O, and N. The C 1s of native ChNCs show that the binding energy of 289.33 and 290.62 belongs to the carbonate region. The C 1s spectrum shows the bonds of carbon with nitrogen. The binding energies of 289.33 and 290.62 belong to the region of carbonyl groups coordinated with water molecules. The binding energy at 288.18 is related to amide bonds and 286.32 is connected with C–N bonds (primary amino groups). The O 1s of native ChNCs show only at 532.9 and 531.5 eV related to the -C-O and -C=O groups in the chemical structure. Partially deacetylated ChNCs show two binding energies at 400.01 and 402.14 that correspond to amide (N-C=O) and primary amino groups (C-N-) of partially deacetylated ChNCs (Figure 4).

 doi:10.20944/preprints202402.0102.v1

From the wide spectrum of native graphene oxide as shown in the figure, only O and C are observed. C 1s of GO@OCF show carbon in the hybridization state sp3 (285 eV) and sp2 (284.5 eV). The peak of carbon in the sp2 state indicates a strong asymmetry as expected with a high proportion of C-O bonds. The different binding energies at 284.5, 286.67, 288.24 and 285 eV correspond to C=C, C-O, COOH, and C-C/C-H, respectively.

Oxidized carbon fibers coated with native graphene oxide (GO@OCF) are shown in Figure 4. As expected from the wide-spectrum data, C, O and Na peaks were observed. The presence of a sodium hydroxide peak is due to the neutralization of OCF with NaOH after the oxidation step to form a salt form (-COONa). The C 1s spectrum shows carbon in two hybridization states as in the native GO spectrum. However, the contribution of C-O bonds decreases in comparison with that of pure GO. The spectrum contains the bonds C=O and ester groups. A new ester group appeared in the C 1s spectrum of GO@OCF at 288.42 eV belonging to carbon in the ester groups due to the esterification reaction between GO and OCF. The intensity of C-O groups of GO@OCF was decreased compared with native GO due to the interaction between OCF and GO.

From the wide spectrum of GO/ChNCs adduct@OCF only C, O, and the N peaks appeared, and peaks were peaks for Na as well. C 1s of GO/ChNCs adduct@OCF show different bending energies at 284.24, 285, 285.6, 286.62, 288.07, 289.41 corresponding to C = C, C-C/CH, C-OH, C-O-, N-C=O-/ COO- and carbon binding with water molecules. From the C 1s spectrum, we could conclude that an esterification/amidation reaction could occur between the functional group of GO/ChNCs adduct and groups of OCF. From the N 1s spectrum of the GO/ChNCs adduct@OCF, only the N-C=O peak appeared and no C-N peak for free amino groups of partially deacetylated ChNCs. From both C 1 and O 1 of GO/ChNCs adduct@OCF, both esterification and amidation reactions could occur between GO/ChNCs adduct and OCF (Figure 4). From FTIR spectra, we can conclusle that the chemical bonding between GO and ChNCs not only via esterification but also via amidation reaction between functional groups of both GO and ChNCs.

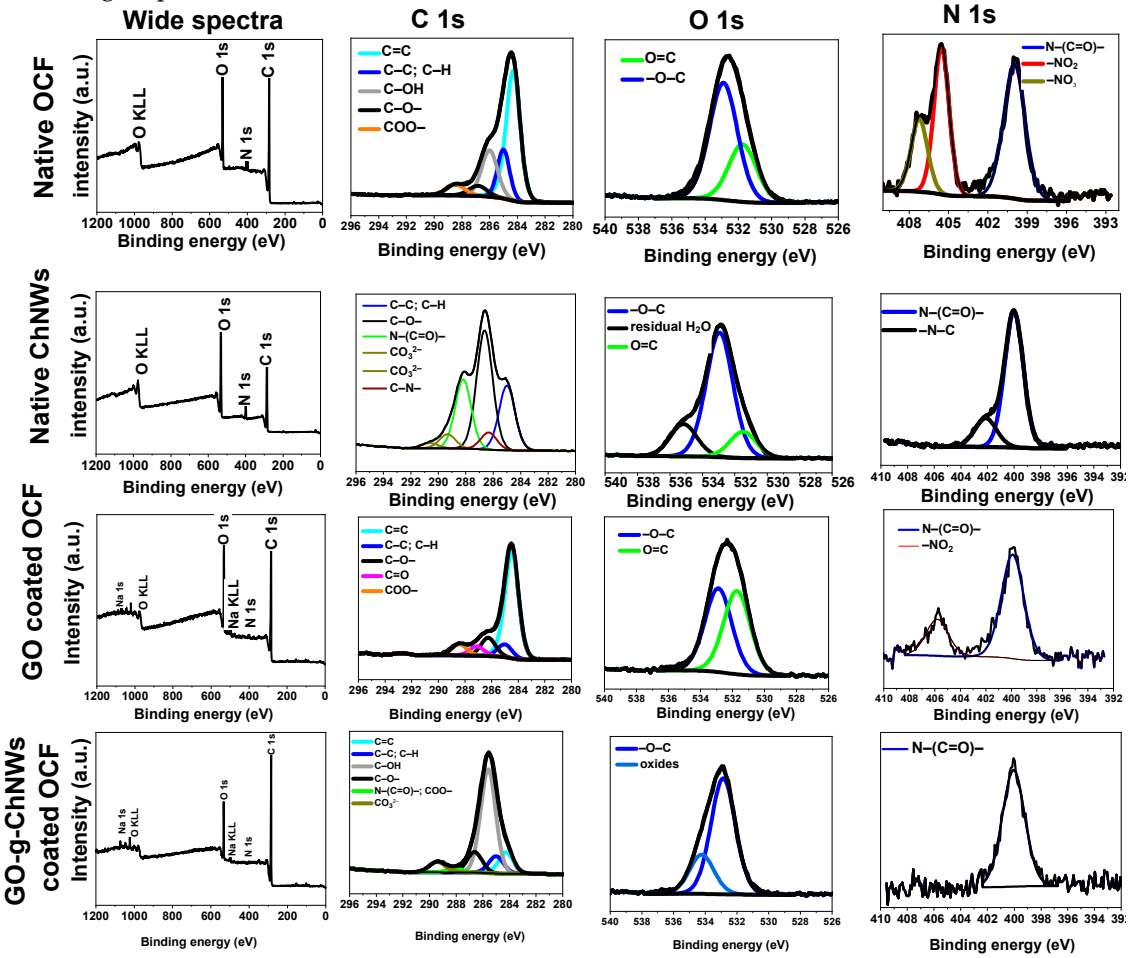

 doi:10.20944/preprints202402.0102.v1

Figure 4. XPS of OCF, ChNCs and GO/ChNCs adduct30 Notes: 5 mg/ml, 10 min, 5 eV, pH 3.5, rt.

3.2. Effect of the GO/ChNCs adduct composition and EPD variations on the structure of the coating

The systematic evaluation of the degree of ChNCs/GO interactions/bonding on the OCF coating was combined with variations of the EPD conditions to obtain complete information about this process up to now not studied. From Figures 5 and S2, S3 follows the marked effect of pH, voltage, and GO/ChNCs adduct concentration on the homogeneity and thickness of the coating. Figure 5 shows the important effect of pH; at lower pH, the OCF was coated with compact homogeneous layers using adducts of all DDA (Figure 5a–c). At neutral pH, the compact layer of the adducts shows small aggregation on the OCF surface, different for respective DDA. At pH 11, the thickness of the coating was small compared to pH 3.4, with high aggregation on the OCF surface mainly for 5 and 30% DDA (Figure 5g–i).

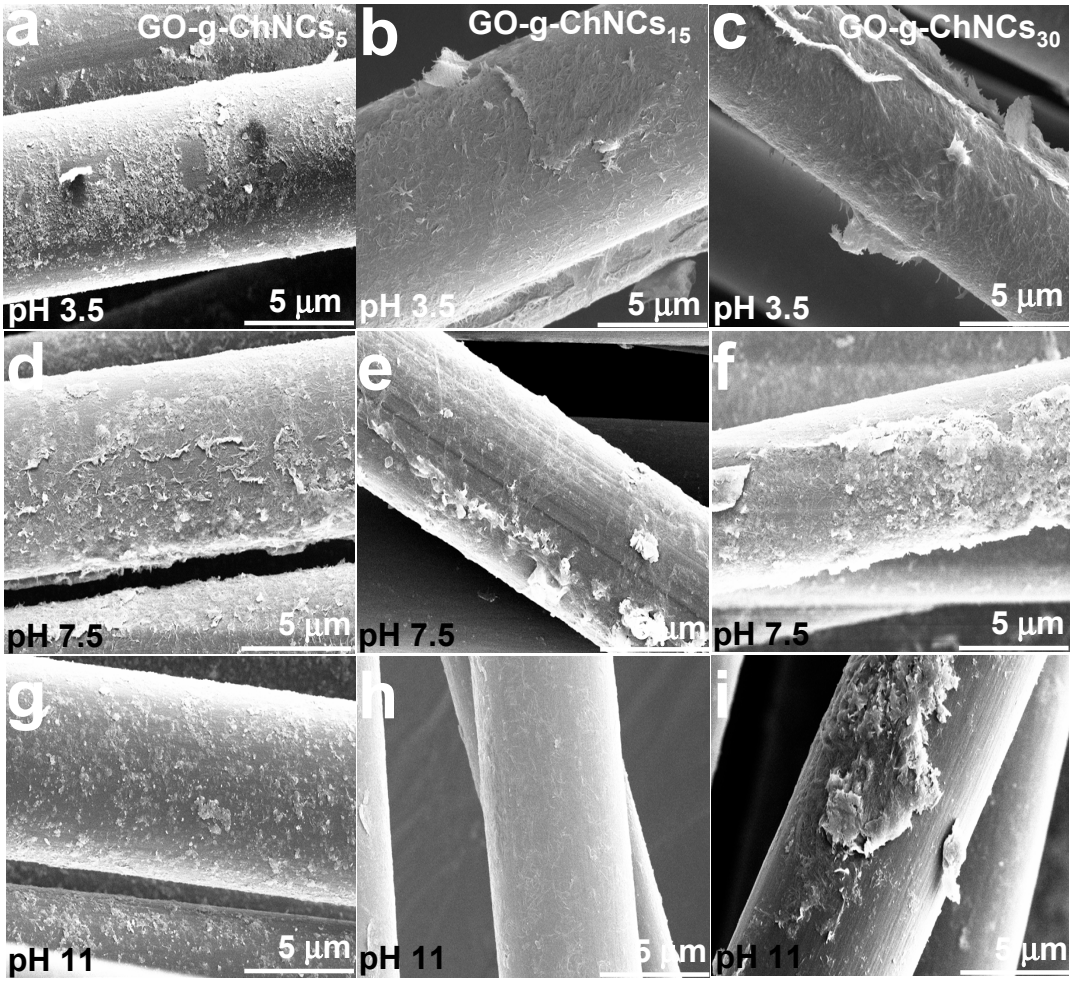

Figure 5. SEM images showing effects of pH and DDA percentages on the OCF coating efficiency using GO/ChNC. Notes: Voltage = 5 V; adduct concentration = 5 mg/ml; coating time 20 min.

The most homogeneous coating for GO/ChNC$_{15}$ adduct at all pH confirms the effect of DDA on the structure of the adduct. This fact was also indirectly indicated by the rheology of the water suspensions as well; see the diffrences in G′ of the adducts with different DDA (5, 30 %, Figure S1b)

Due to the relatively large size of the adducts and the expected high charge density together with the related slower assembly/ordering, unlike the GO-g-polymer chain or polydopamine coated GO, the best deposition occurs at a lower voltage [46]. As we can see, the low applied voltage (5 V) obtained was more homogeneous and compact layered of GO/ChNCs adduct (Figure S1) compared to the high applied voltage (20 V). Figure S3 shows the effect of adduct concentration on the homogeneity of the OCF coating. As we can see, at lower concentrations, the coating had a

 doi:10.20944/preprints202402.0102.v1

heterogeneous distribution on the fiber surface up to (1 mg/ml). A more compact and homogeneous layered was obtained on the OCF surface at higher adduct concentrations.

From Figure 6. it follows that the effect of DDA and thus the structure, size, and charge density of the adduct strongly influences the thickness of the EPD layer; see the growing tendency with DDA with markedly most considerable thickness for 30 % DDA with about 120-160 nm.

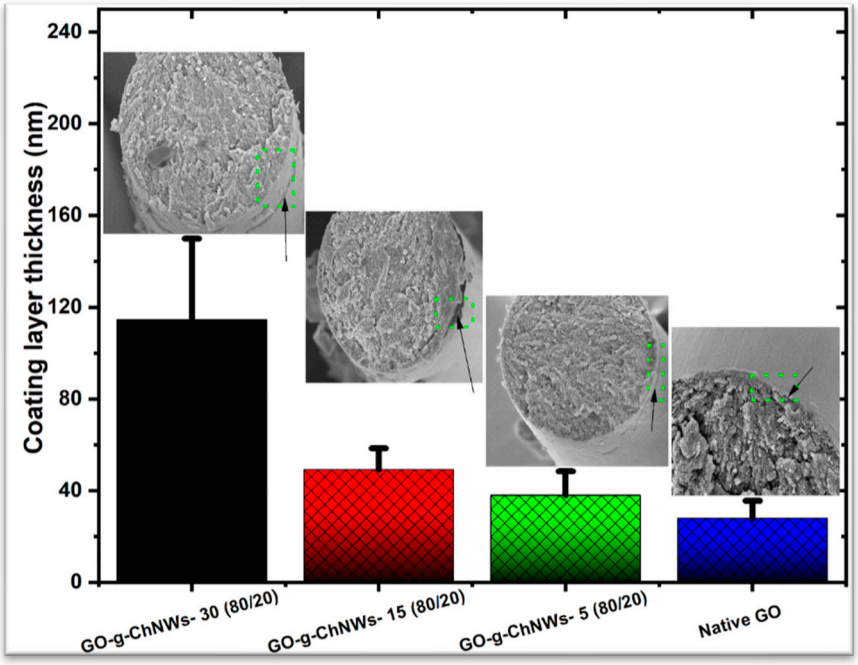

Figure 6. Effects of DDA on the coating thickness of GO/ChNCs adduct (80/20). Notes: 10 min, 5 eV, DDA 30 %, pH 3.5, rt.

3.3. Short-beam testing (SBS)

Based on systematic evaluation of EPD conditions on the homogeneity and composition of the coating (see above), we have used fibers with the most 'compact' coating, i.e., prepared using GO/ChNCs adduct with a concentration of 5 mg/ml, pH ~3.5, voltage 5 V, and coating time 10 min for preparation of composite short beam samples. The GO / ChNCs ratio was 95/5, 90/10, 80/20 and 50/50 were used with different DDA of ChNCs (5, 15, 30 %), respectively. The thickness of the coating ranged between 40-120 nm (Figure 6); due to the very low effect of the coating thickness in this range on composite parameters, indicated both experimentally and by FEA modeling in our previous paper [46], we did not focus on achieving an identical coating size for the respective adducts in this study. Here, it is important to note that testing of beam samples made from a 'bundle' of fibers, unlike those from plies (laminate samples), has low relevancy to interlaminar shear strength (ILSS). The main purpose of this test was to evaluate the possible unfavorable effect of coating on basic mechanical properties, which is a limiting factor in most existing solutions using tough coatings [34,53]. At the same time, the first results of a laminate plate made from 30 layers of carbon cloth with an interlayer based on EPD of (relatively rigid) polydopamine PDA-coated GO indicate a positive effect on delamination resistance. Therefore, we can expect a similar performance for the system studied.

From Figure 7 showing results of the SBS testing follows the relatively marked effect of DDA of ChNC on the modulus with a strong dependence on the GO/ChNCs ratio, which is reflected in various trends for each composition. In the case of nacre-like composition, that is, 95/5 and 90/10 GO/ChNCs ratios, we can see the most marked modulus increase against the samples with GO-coated fibers. Therefore, with all DDA we can undoubtedly expect the formation of favorable brick-and-mortar structures reported by others in the case of planar samples (films) [1,3,4,6]. Interestingly, in the case of 95/5 composition, the modulus decreases with DDA, whereas with 90/10 ratio it slightly increases.

 doi:10.20944/preprints202402.0102.v1

For 80/20 and 50/50 GO/ChNCs ratios, we can see more marked modulus variations with DDA, that is, the maximal value (exceeding GO) at 15 % DDA and 30 % DDA, respectively. Especially in the case of 50/50 adducts, the expected relatively higher content of ChNCs-amines at the interface with a higher potential for bonding with the matrix may be of importance. This is confirmed by the most marked matrix layer attached to the OCF coated also with GO/ChNCs$_{30}$ 90/10 adduct (Figure 8). At the same time, the effect of DDA on the short beam strength (SBS) was less pronounced, with values comparable to those of the GO coating. Slightly higher values against GO were found for 95/5 and 90/10 interlayers containing ChNCs with 15 % DDA. This also indicates a similar brick-and-mortar structure. Figure 6 further follows practically no effect of DDA for an 80/20 ratio, while a slight enhancement with 30 % DDA for a 50/50 ratio may correspond to the highest potential for bonding with the epoxy matrix (Figure 7). The short-beam testing results indicate that all coating types do not cause unbearable decrease of composite parameters, so can be used for further research focused on revealing their effect on delamination resistance using planar multilayered laminates

Finally, from the observation of fracture surfaces of composites with OCF coated with GO and GO/ChNC 90/10 adducts (Figure 8) follows practically no matrix presented on the surface of GO coated CF whereas relatively marked matrix layer on GO/ChNC adducts coated OCF indicate expected bonding of ChNW amines to epoxy matrix. Increase in the size and thickness of the attached matrix fragments with ChNC with higher DDA and thus content of primary amines corresponds to higher reactivity of primary amines with epoxy groups of epoxy resin in comparison with secondary amines [54]. At the same time, practically no correspondece of this bonding to SBS strength indicate that effect of EPD coating on strength dominates

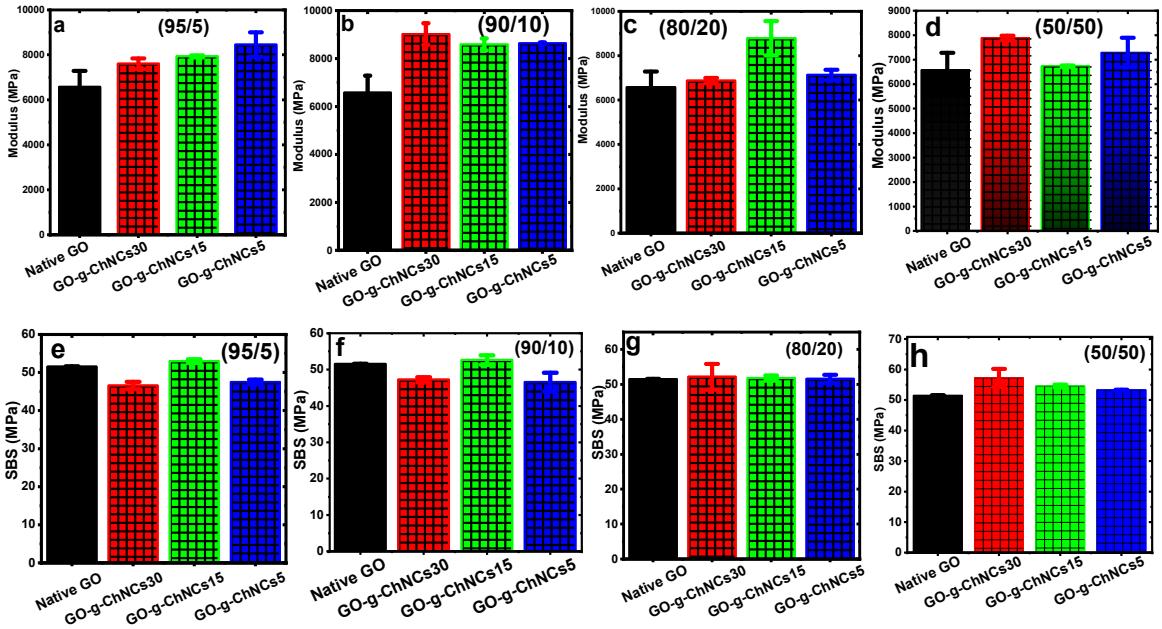

Figure 7. Three-point short-beam bending test of composite samples.

 doi:10.20944/preprints202402.0102.v1

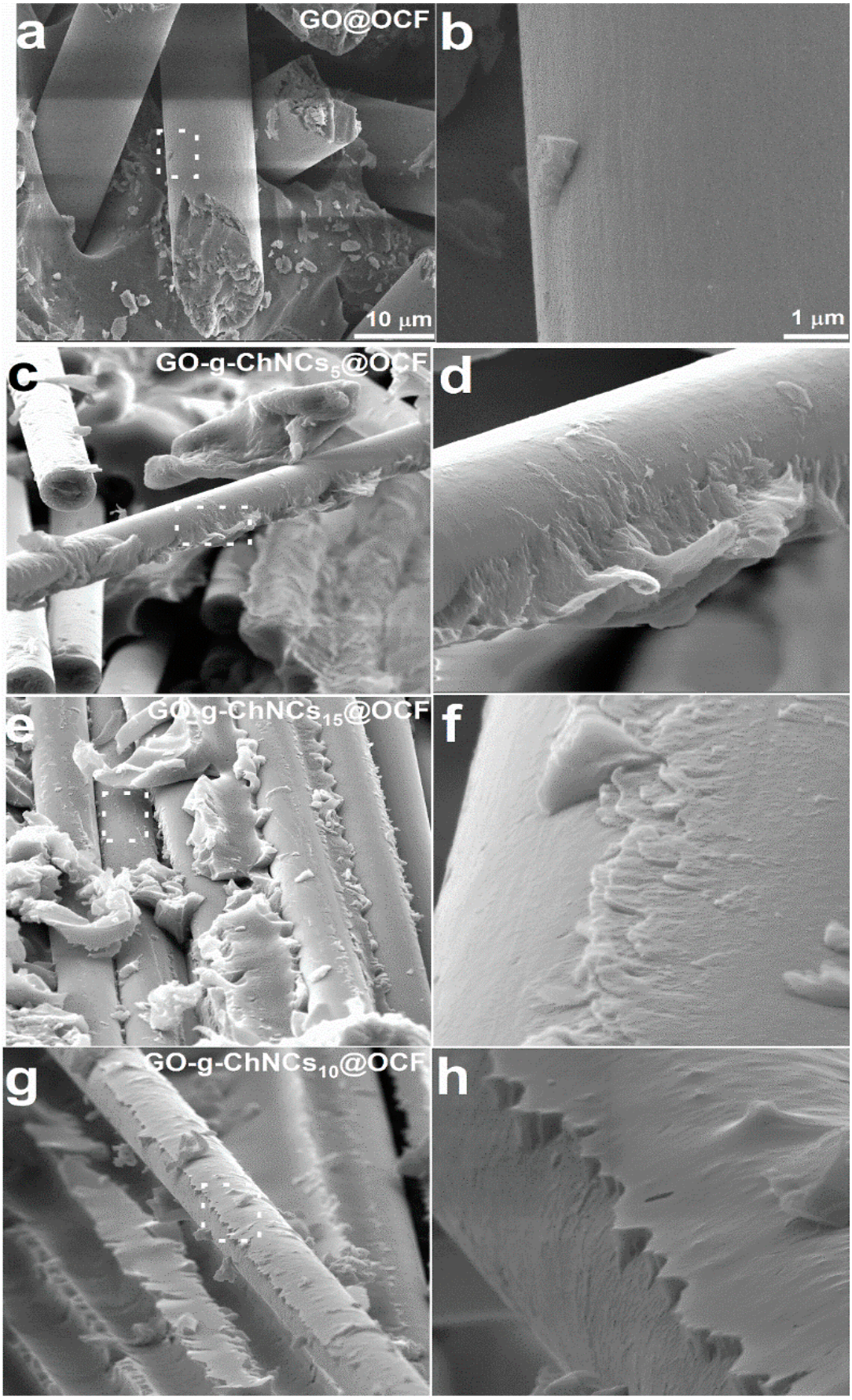

Figure 8. SEM of fractured composite with OCF coated with native GO(a, b); GO/ChNCs$_5$ adduct (c, d); GO/ChNCs$_{15}$ adduct (e, f) and GO/ChNCs$_{30}$ adduct (g, h). GO-ChNCs$_{30}$ (90/10 GO/ChNC ratio in all cases).

4. Conclusions

Chitin nanocrystals (ChNCs) with different DDAs were prepared and used for preparation of adducts with graphene oxide (GO) with different GO/ChNCs ratios Their structure was confirmed using different techniques, such as FTIR, XRD, XPS, and DLS. The results indicate that the formation of GO/ChNCs adduct enables an effective electrophoretic coating of the OCFs to form a rigid tough interface. We have revealed crucial parameters controlling the EPD and homogeneity of the coatings (pH, concentration, voltage). having comparable mechanical parameters, which are also confirmed by the negligible effect of such an interface on the SBS and the modulus of composites. We expect that especially coating with a nacre-like composition, i.e. using GO/ChNCs adduct with 95/5 and 90/10 ratio, can provide a rigid, tough interface with fair potential to increase delamination resistance.

Supplementary Materials: The following supporting information can be downloaded at the website of this paper posted on Preprints.org.

Acknowledgments: This work was supported by Ministry of Education Youth and Sports of the Czech Republic (Grant LUAUS 23004).

Supporting information: Rheological characterization, SEM images of single coated fibers.

References

1. Y. Zhang, S. Gong, Q. Zhang, P. Ming, S. Wan, J. Peng et al., Graphene-based artificial nacre nanocomposites, Chem. Soc. Rev. 45 (2016) 2378–2395. https://doi.org/10.1039/C5CS00258C.
2. L.J. Bonderer, A.R. Studart, L.J. Gauckler, Bioinspired Design and Assembly of Platelet Reinforced Polymer Films, Science 319 (2008) 1069–1073. https://doi.org/10.1126/science.1148726.
3. U.G.K. Wegst, H. Bai, E. Saiz, A.P. Tomsia, R.O. Ritchie, Bioinspired structural materials. Nat. Mater. 14 (2015) 23–36. https://doi.org/10.1038/nmat4089.
4. S. Wan, J. Peng, Y. Li, H. Hu, L. Jiang, Q. Cheng, Use of Synergistic Interactions to Fabricate Strong, Tough, and Conductive Artificial Nacre Based on Graphene Oxide and Chitosan, ACS Nano 9 (2015) 9830–9836. https://doi.org/10.1021/acsnano.5b02902.
5. R.Z. Wang, Z. Suo, A.G. Evans, N. Yao, I.A. Aksay, Deformation mechanisms in nacre, J. Mater. Res. 16 (2001) 2485–2493. http://dx.doi.org/10.1557/JMR.2001.0340.
6. K. Chen, X. Tang, Y. Yue, H. Zhao, L. Guo, Strong and Tough Layered Nanocomposites with Buried Interfaces, ACS Nano 10 (2016) 4816–4827. https://doi.org/10.1021/acsnano.6b01752.
7. J. Duan, S. Gong, Y. Gao, X. Xie, L. Jiang, Q. Cheng, Bioinspired Ternary Artificial Nacre Nanocomposites Based on Reduced Graphene Oxide and Nanofibrillar Cellulose, ACS Appl. Mater. Interfaces 8 (2016) 10545–10550. https://doi.org/10.1021/acsami.6b02156.
8. K. Yao, S. Huang, H. Tang, Y. Xu, G. Buntkowsky, L.A. Berglund et al., Bioinspired Interface Engineering for Moisture Resistance in Nacre-Mimetic Cellulose Nanofibrils/Clay Nanocomposites. ACS Appl. Mater. Interfaces 9 (2017) 20169–20178. https://doi.org/10.1021/acsami.7b02177.
9. M. Li, X. Wang, R. Zhao, Y. Miao, Z. Liu, A novel graphene-based micro/nano architecture with high strength and conductivity inspired by multiple creatures, Sci. Rep. 11 (2021), 1387. https://doi.org/10.1038/s41598-021-80972-8.
10. R. Xiong, H.S. Kim, L. Zhang, V.F. Korolovych, S. Zhang, Y.G. Yingling et al., Wrapping Nanocellulose Nets around Graphene Oxide Sheets, Angew. Chem. Int. Ed. 57 (2018) 8508–8513. https://doi.org/10.1002/anie.201803076.
11. Y. Liu, S.-H. Yu, L. Bergström, Transparent and Flexible Nacre-Like Hybrid Films of Aminoclays and Carboxylated Cellulose Nanofibrils, Adv. Funct. Mater. 28 (2018), 1703277. https://doi.org/10.1002/adfm.201703277.
12. D. Xu, S. Wang, L.A. Berglund, Q. Zhou, Surface Charges Control the Structure and Properties of Layered Nanocomposite of Cellulose Nanofibrils and Clay Platelets, ACS Appl. Mater. Interfaces 13 (2021) 4463–4472. https://doi.org/10.1021/acsami.0c18594.
13. P. Laaksonen, A. Walther, J.-M. Malho, M. Kainlauri, O. Ikkala, M.B. Linder, Genetic Engineering of Biomimetic Nanocomposites: Diblock Proteins, Graphene, and Nanofibrillated Cellulose, Angew. Chem. Int. Ed. 50 (2011) 8688–8691. https://doi.org/10.1002/anie.201102973.

14. L. Huang, C. Li, W. Yuan, G. Shi, Strong composite films with layered structures prepared by casting silk fibroin–graphene oxide hydrogels, Nanoscale 5 (2013) 3780–3786. https://doi.org/10.1039/C3NR00196B.
15. M. Li, P. Xiong, M. Mo, Y. Cheng, Y. Zheng, Electrophoretic-deposited novel ternary silk fibroin/graphene oxide/hydroxyapatite nanocomposite coatings on titanium substrate for orthopedic applications, Front. Mater. Sci. 10 (2016) 270–280. https://doi.org/10.1007/s11706-016-0347-7.
16. W. Zhang, K. Zheng, J. Ren, Y. Fan, S. Ling, Strong, ductile and lightweight bionanocomposites constructed by bioinspired hierarchical assembly, Compos. Commun. 17 (2020) 97–103. https://doi.org/10.1016/j.coco.2019.11.017.
17. T.H. Tran, H.-L. Nguyen, D.S. Hwang, J.Y. Lee, H.G. Cha, J.M. Koo et al., Five different chitin nanomaterials from identical source with different advantageous functions and performances, Carbohydr. Polym. 205 (2019) 392–400. https://doi.org/10.1016/j.carbpol.2018.10.089.
18. R.M. Abdelrahman, A.M. Abdel-Mohsen, M. Zboncak, J. Frankova, P. Lepcio, L. Kobera et al., Hyaluronan biofilms reinforced with partially deacetylated chitin nanowhiskers: Extraction, fabrication, in-vitro and antibacterial properties of advanced nanocomposites, Carbohydr. Polym. 235 (2020), 115951. https://doi.org/10.1016/j.carbpol.2020.115951.
19. I. Kelnar, J. Kovářová, G. Tishchenko, L. Kaprálková, E. Pavlová, F. Carezzi et al., Chitosan/Chitin nanowhiskers composites: effect of plasticisers on the mechanical behaviour, J. Polym. Res. 22 (2015), 5. https://doi.org/10.1007/s10965-014-0648-4.
20. A.J. Uddin, M. Fujie, S. Sembo, Y. Gotoh, Outstanding reinforcing effect of highly oriented chitin whiskers in PVA nanocomposites, Carbohydr. Polym. 87 (2012) 799–805. https://doi.org/10.1016/j.carbpol.2011.08.071.
21. C. Wang, J. Li, S. Sun, X. Li, F. Zhao, B. Jiang et al., Electrophoretic deposition of graphene oxide on continuous carbon fibers for reinforcement of both tensile and interfacial strength, Compos. Sci. Technol. 135 (2016) 46–53. https://doi.org/10.1016/j.compscitech.2016.07.009.
22. J. Jiang, X. Yao, C. Xu, Y. Su, L. Zhou, C. Deng, Influence of electrochemical oxidation of carbon fiber on the mechanical properties of carbon fiber/graphene oxide/epoxy composites, Compos. Pt. A-Appl. Sci. Manuf. 95 (2017) 248–256. https://doi.org/10.1016/j.compositesa.2017.02.004.
23. C. Wang, Y. Li, L. Tong, Q. Song, K. Li, J. Li et al., The role of grafting force and surface wettability in interfacial enhancement of carbon nanotube/carbon fiber hierarchical composites, Carbon 69 (2014) 239–246. https://doi.org/10.1016/j.carbon.2013.12.020.
24. Q. Zhang, D. Jiang, L. Liu, Y. Huang, J. Long, G. Wu et al., Effects of Graphene Oxide Modified Sizing Agents on Interfacial Properties of Carbon Fibers/Epoxy Composites. J. Nanosci. Nanotechnol. 15 (2015) 9807–9811. https://doi.org/10.1166/jnn.2015.10625.
25. R.L. Zhang, B. Gao, Q.H. Ma, J. Zhang, H.Z. Cui, L. Liu, Directly grafting graphene oxide onto carbon fiber and the effect on the mechanical properties of carbon fiber composites, Mater. Des. 93 (2016) 364–369. https://doi.org/10.1016/j.matdes.2016.01.003.
26. H. Qian, E.S. Greenhalgh, M.S.P. Shaffer, A. Bismarck, Carbon nanotube-based hierarchical composites: a review. J. Mater. Chem. 20 (2010) 4751–4762. https://doi.org/10.1039/C000041H.
27. Y. Li, Q. Peng, X. He, P. Hu, C. Wang, Y. Shang et al., Synthesis and characterization of a new hierarchical reinforcement by chemically grafting graphene oxide onto carbon fibers, J. Mater. Chem. 22 (2012) 18748–18752. https://doi.org/10.1039/C2JM32596A.
28. A. Asadi, M. Miller, R.J. Moon, K. Kalaitzidou, Improving the interfacial and mechanical properties of short glass fiber/epoxy composites by coating the glass fibers with cellulose nanocrystals, Express Polym. Lett. 10 (2016) 587–597. https://doi.org/10.3144/expresspolymlett.2016.54.
29. B.E.B. Uribe, E.M.S. Chiromito, A.J.F. Carvalho, J.R. Tarpani, Low-cost, environmentally friendly route for producing CFRP laminates with microfibrillated cellulose interphase. Express Polym. Lett. 11 (2017) 47–59. https://doi.org/10.3144/expresspolymlett.2017.6
30. M.D. Reale Batista, L.T. Drzal, Carbon fiber/epoxy matrix composite interphases modified with cellulose nanocrystals, Compos. Sci. Technol. 164 (2018) 274–281. https://doi.org/10.1016/j.compscitech.2018.05.010.
31. J.U. Lee, B. Park, B.-S. Kim, D.-R. Bae, W. Lee, Electrophoretic deposition of aramid nanofibers on carbon fibers for highly enhanced interfacial adhesion at low content. Compos. Pt. A-Appl. Sci. Manuf. 84 (2016) 482–489. https://doi.org/10.1016/j.compositesa.2016.02.029.
32. B. Zhang, T. Lian, X. Shao, M. Tian, N. Ning, L. Zhang et al., Surface Coating of Aramid Fiber by a Graphene/Aramid Nanofiber Hybrid Material to Enhance Interfacial Adhesion with Rubber Matrix, Ind. Eng. Chem. Res. 60 (2021) 2472–2480.
33. M.R. Wisnom, The role of delamination in failure of fibre-reinforced composites. Philos. Trans. R. Soc. A-Math. Phys. Eng. Sci. 370 (2012) 1850–1870. https://doi.org/10.1098/rsta.2011.0441.
34. J.-F. Gerard, Characterization and role of an elastomeric interphase on carbon fibers reinforcing an epoxy matrix. Polym. Eng. Sci. 28 (1988) 568–577. https://doi.org/10.1002/pen.760280905.
35. B.D. Agarwal, R.K. Bansal, Effect of an interfacial layer on the properties of fibrous composites: A theoretical analysis, J. Fiber Sci. Technol. 12 (1979) 149–158. https://doi.org/10.1016/0015-0568(79)90027-7.

36. S. Lee, S. Ryu, Theoretical study of the effective modulus of a composite considering the orientation distribution of the fillers and the weakened interface, Eur. J. Mech. A/Solids 72 (2018) 79–89. https://doi.org/10.1016/j.euromechsol.2018.02.008.
37. A. Kausar, M. Siddiq, Epoxy composites reinforced with multi-walled carbon nanotube/poly(ethylene glycol)methylether-coated aramid fiber, J. Polym. Eng. 36 (2016) 465–471. https://doi.org/10.1515/polyeng-2015-0191.
38. X. Yao, X. Gao, J. Jiang, C. Xu, C. Deng, J. Wang, Comparison of carbon nanotubes and graphene oxide coated carbon fiber for improving the interfacial properties of carbon fiber/epoxy composites, Compos. B Eng. 132 (2018) 170–177. https://doi.org/10.1016/j.compositesb.2017.09.012.
39. P. Wang, J. Yang, W. Liu, X.-Z. Tang, K. Zhao, X. Lu et al., Tunable crack propagation behavior in carbon fiber reinforced plastic laminates with polydopamine and graphene oxide treated fibers, Mater. Des. 113 (2017) 68–75. https://doi.org/10.1016/j.matdes.2016.10.013.
40. F. De Luca, G. Sernicola, M.S.P. Shaffer, A. Bismarck, "Brick-and-Mortar" Nanostructured Interphase for Glass-Fiber-Reinforced Polymer Composites, ACS Appl. Mater. Interfaces 10 (2018) 7352–7361. https://doi.org/10.1021/acsami.7b16136.
41. X. Yang, H. Du, S. Li, Z. Wang, L. Shao, Codepositing Mussel-Inspired Nanohybrids onto One-Dimensional Fibers under "Green" Conditions for Significantly Enhanced Surface/Interfacial Properties. ACS Sustain. Chem. Eng. 6 (2018) 4412–4420. https://doi.org/10.1021/acssuschemeng.8b00290.
42. L. Jin, M. Zhang, L. Shang, L. Liu, M. Li, Y. Ao, A nature-inspired interface design strategy of carbon fiber composites by growing brick-and-mortar structure on carbon fiber. Compos. Sci. Technol. 200 (2020), 108382. https://doi.org/10.1016/j.compscitech.2020.108382.
43. J. Wang, S. Zhou, J. Huang, G. Zhao, Y. Liu, Interfacial modification of basalt fiber filling composites with graphene oxide and polydopamine for enhanced mechanical and tribological properties, RSC Adv. 8 (2018) 12222–12231. https://doi.org/10.1039/C8RA00106E.
44. D.C. Marcano, D.V. Kosynkin, J.M. Berlin, A. Sinitskii, Z. Sun, A. Slesarev et al., Improved Synthesis of Graphene Oxide, ACS Nano 4 (2010) 4806–4814. https://doi.org/10.1021/nn1006368.
45. I. Kelnar, L. Kaprálková, P. Němeček, J. Dybal, R.M. Abdel-Rahman, M. Vyroubalová et al., The Effects of the Deacetylation of Chitin Nanowhiskers on the Performance of PCL/PLA Bio-Nanocomposites, Polymers 15 (2023), 3071. https://doi.org/10.3390/polym15143071.
46. I. Kelnar, L. Kaprálková, P. Němeček, M. Janata, J. Dybal, J. Svoboda et al., Nature-mimicking rigid tough interface in fibrous composites: Effect of polymer/GO combination. Mater. Today Commun. 33 (2022), 104883. https://doi.org/10.1016/j.mtcomm.2022.104883.
47. Q. Wu, X. Yang, Z. Ye, H. Deng, J. Zhu, Dopamine-dependent graphene oxide modification and its effects on interfacial adhesion of carbon fiber composites, Surf. Interfaces 31 (2022), 102086. https://doi.org/10.1016/j.surfin.2022.102086.
48. A.M. Abdel-Mohsen, R.M. Abdel-Rahman, I. Kubena, L. Kobera, Z. Spotz, M. Zboncak et al., Chitosan-glucan complex hollow fibers reinforced collagen wound dressing embedded with aloe vera. Part I: Preparation and characterization, Carbohydr. Polym. 230 (2020), 115708. https://doi.org/10.1016/j.carbpol.2019.115708.
49. A.S. Aly, A.M. Abdel-Mohsen, R. Hrdina, A. Abou-Okeil, Preparation and Characterization of Polyethylene Glycol/Dimethyl Siloxane Adduct and Its Utilization as Finishing Agent for Cotton Fabric, J. Nat. Fibers. 8 (2011) 176–188. https://doi.org/10.1080/15440478.2011.602243.
50. Z. Lin, Y. Ma, C. Hu, Q. Zhang, Molecular intercalated graphene oxide with finely controllable interlayer spacing for fast dye separation, Colloids Surf. A: Physicochem. Eng. Asp. 677 (2023), 132437. https://doi.org/10.1016/j.colsurfa.2023.132437.
51. S. Dong, B. Wang, D. Liu, M. He, M. Chen, J. Zhao et al., Tailoring the interlayer channel structure of graphene oxide membrane with conjugated cationic dyes for butanol dehydration, Sep. Purif. Technol. 325 (2023), 124728. https://doi.org/10.1016/j.seppur.2023.124728.
52. W.L. Xu, C. Fang, F. Zhou, Z. Song, Q. Liu, R. Qiao et al., Self-Assembly: A Facile Way of Forming Ultrathin, High-Performance Graphene Oxide Membranes for Water Purification, Nano Lett. 17 (2017) 2928–2933. https://doi.org/10.1021/acs.nanolett.7b00148.
53. N. Zheng, Y. Huang, H.-Y. Liu, J. Gao, Y.-W. Mai, Improvement of interlaminar fracture toughness in carbon fiber/epoxy composites with carbon nanotubes/polysulfone interleaves, Compos. Sci. Technol. 140 (2017) 8–15. https://doi.org/10.1016/j.compscitech.2016.12.017.
54. C.C. Riccardi, H.E. Adabbo, R.J.J. Williams, Curing reaction of epoxy resins with diamines, J. Appl. Polym. Sci. 29 (1984) 2481–2492. https://doi.org/10.1002/app.1984.070290805.